EMIR Band 4 Commissioning Report
Draft version V2.3

April, 5th, 2010
C. Kramer, J. Penalver, S. Navarro

ABSTRACT. For the first time since more than 10 years, the telescope is equipped again with a line receiver for the 0.8 mm window (the dual polarization band E330 of EMIR). At 340 GHz, the HPBW is $7.5''$ and the aperture efficiency is 29%. These values hold near the optimium elevation of about 50 deg. At lower and at higher elevations, the beam broadens and becomes slightly eliptical. The aperture efficiency degrades significantly at 30 deg elevation. We observed a degradation of the lateral focus at low elevations, when the dish was illuminated by the sun. Observations of the gain elevations dependence at night time are pending. The total surface rms is estimated to be $64\,\mu$m, at the optimum elevation, using also E1 data and the Ruze formula.

The forward efficiency is 81%, measured with the porexpan vertex radome in place. It increases to 86% when the radome is removed. This 6% improvement is consistent with direct measurements of the radome transmission.

Lunar edge scans show the known diffraction ring below -15 dB, explained by panel buckling. The alignment between E1 and E3 is about $0.3''$. The focus difference between E1 and E3 is 0.21 mm.

Band 4 has been successfully tuned over most of the frequency range between 260 and 351 GHz. Two small frequency intervals below 350 GHz, show instabilities. The present Local Oscillator does not allow to reach higher frequencies. The vertical polarisation shows a much higher noise than the horizontal polarisation, as seen in continuum observations.

Here, we summarize the commissiong results of band 4 of EMIR at the IRAM 30m telescope, conducted in winter 2009/10. The local oscillator installed with EMIR for band 4 in April 2009, did not have sufficient power above 330 GHz and other problems. On November, 17th, 2009, a new and more powerful local oscillator for band 4 was installed, allowing to finish E3 commissioning.

E3 has been used for regular observations since the start of the winter semester 2009/2010 on December, 1st, 2009, without encountering any specific problems.

1 Receiver Tuning

Sky frequencies between 260 GHz upto 351 GHz were tuned. Higher frequencies can, at present, not be reached.

At 330 GHz LO frequency (± 0.6 GHz) the LO cannot be locked. At 339 GHz LO frequency (± 1.5 GHz) the tuning is instable. This instability is an intermittent problem, changing from one day to the next for unknown reasons! The observer may avoid problems at these LO frequencies, by changing the sideband of interest.

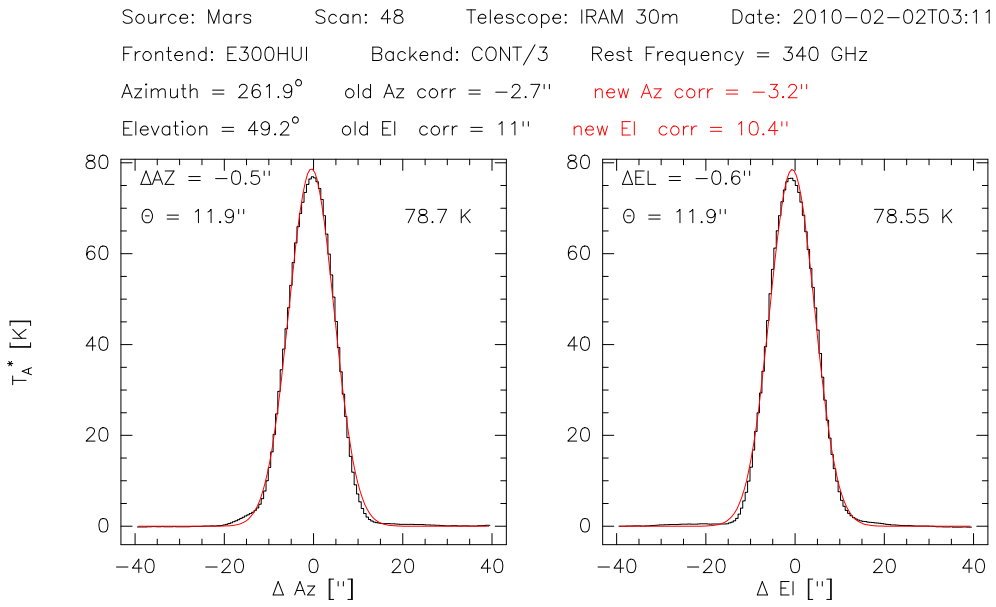

Figure 1: Mars pointing scan at 340 GHz, near the optimum elevation, observed on 02-Feb-2010.

2 Continuum observations

2.1 Telescope beam widths and efficiencies

Figure 1 shows the result of a cross scan on Mars taken at the "optimum" elevation of $49°$ on 02-Feb-2010. Deviations from a Gaussian beam are hardly discernable, at the linear plotting scale,

In the following, we show the results of observations taken on November, 23./24., 2009, under excellent weather conditions of an amount of precipitable water vapor (pwv) of 1 mm.

All observations described in this report, were taken with the vertex porexpan membrane in place, as this is the standard setting for all observations. In section 2.7, we describe tests without membrane.

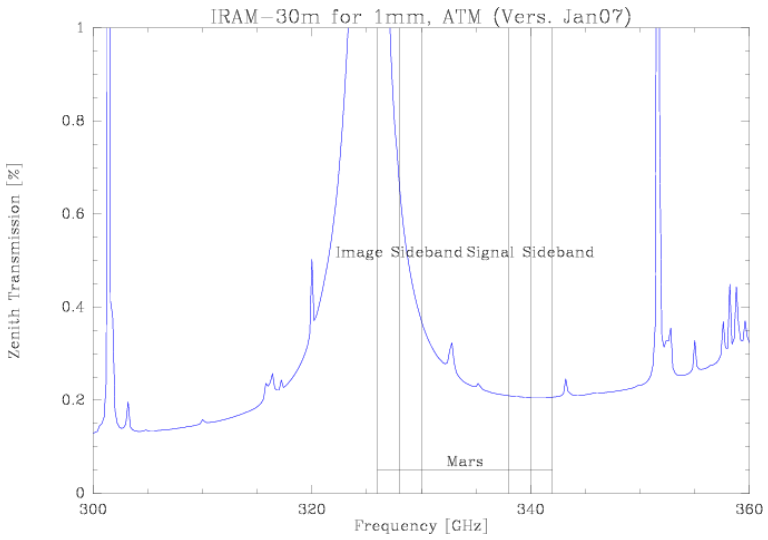

Figure 2: Atmospheric transmission near 340 GHz.

Table 1 shows the derived forward efficiency at 340 GHz. This value is based on 11 skydips. For the mean atmospheric temperature, the CLASS header information from the chopper wheel calibration was used.

Table 1: Telescope half power beam width and forward, main beam, and aperture efficiencies. Here, we assume a Gaussian beam and $B_{\rm eff} = 1.21\, A_{\rm eff}$ (Baars 2007).

Frequency GHz]	HPBW [″]	$F_{\rm eff}$ [%]	$B_{\rm eff}$ [%]	$A_{\rm eff}$ [%]	Date
340	7.5	81 ± 1	35 ± 2	29 ± 2	23./24.-Nov-09 (JP)

Table 1 also shows the aperture efficiency and half power beam width (HPBW), derived from Mars observations on 24-Nov-2009 near the optimum elevation of $\sim 49°$. Mars had a diameter of $9.3''$. The new atmospheric model ATM09 was used for the calibration. It takes into account the atmospheric line in the image band near 325 GHz (Fig. 2).

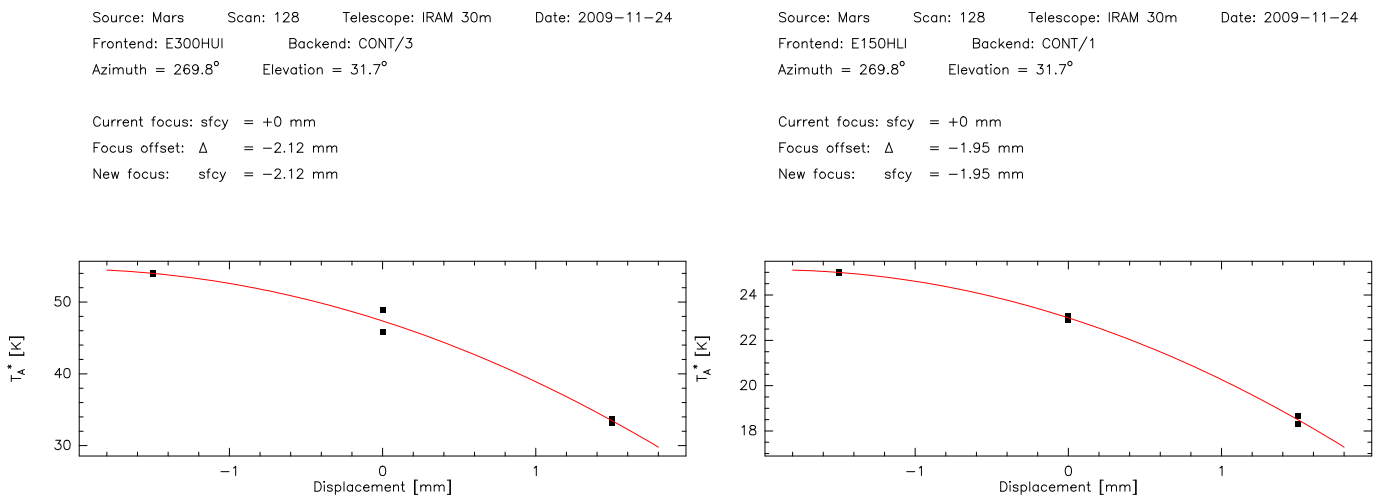

Figure 3: Focus scan on Mars in Y-direction, taken at 31 ° elevations, in the morning hours of 24-Nov-2009. Left: Scan at 340 GHz. Right: Scan at 145 GHz.

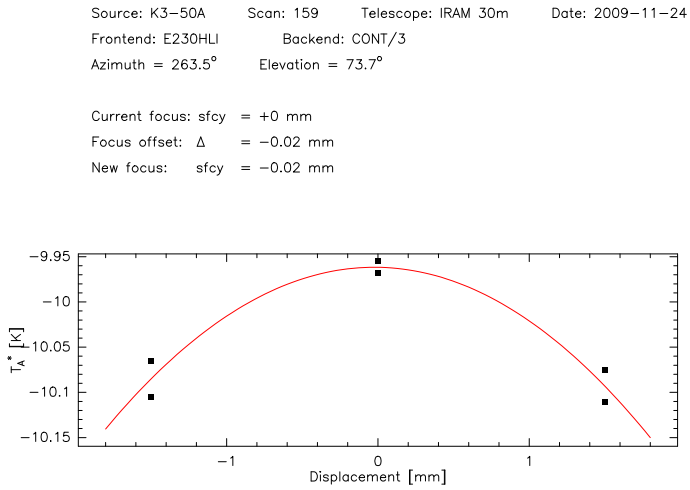

Figure 4: A y-focus scan at 70 degree elevation with E2, taken in the afternoon of 24-Nov-2009, shows no offset.

2.2 Lateral focus

Lateral focus scans were conducted, just before the efficiency measurements at 30 deg elevation (Figs. 3,4). These scans show a focus offset at 340 and 145 GHz at low elevations, while there is no offset at high elevations. The offsets were not corrected for. These findings indicate that the lateral focus is not stable and changes with sun angle, or elevations. At the efficiency observations were not corrected for lateral focus offsets, the gain-elevation curves which are discussed below are affected. Lateral focus scans are usually not conducted by the observers, as these very sensitive observations need especially stable weather conditions, and a strong source. This of course relies on the assumption that the lateral focus does not change.

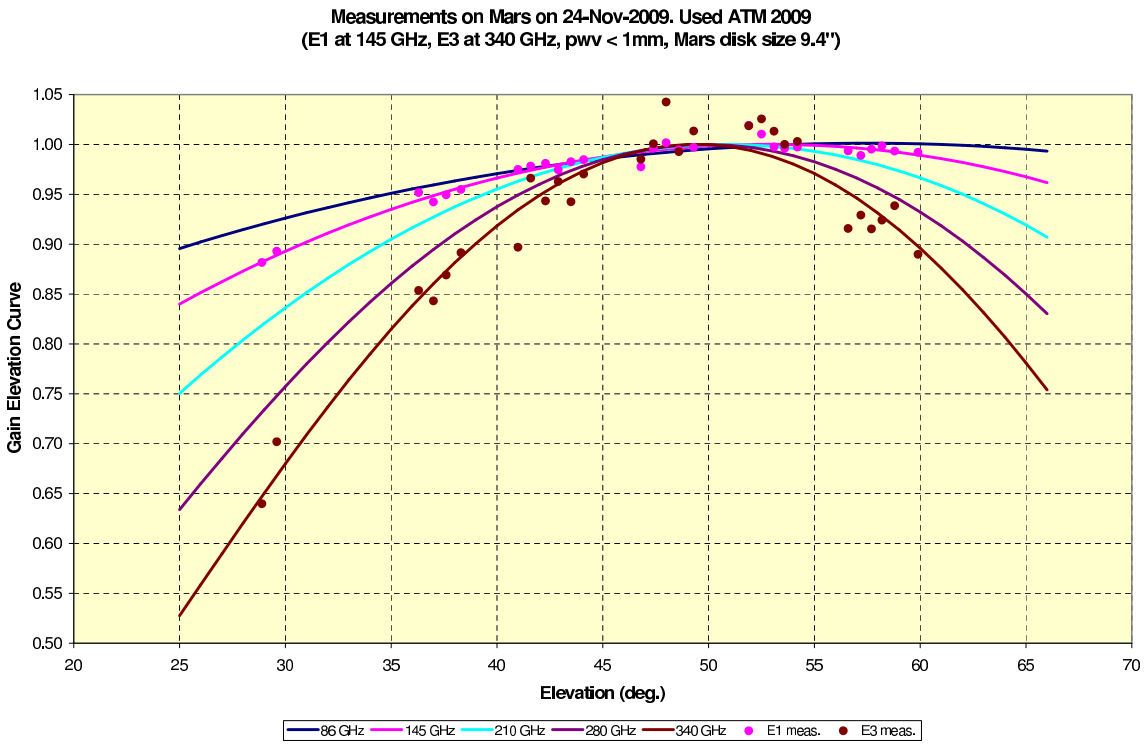

Figure 5: Variation of the aperture efficiencies with elevation, at 145 GHz and at 340 GHz, observed on 24-Nov-2009, together with fitted gain-elevation curves. The curves at 86, 210, 280 GHz are extrapolated from the fit of the surface accuracy shown in Figure 7. All values have been normalized to the fitted peak aperture efficiency $A_{\rm eff}$ at 49 deg elevation.

2.3 Gain elevation curve: efficiencies

Figure 5 shows the variation of the aperture efficiency with elevation, between 28° and 60°.

Note that the gain-elevation curve peaks near 49° elevation, as previously noted, though the telescope had been adjusted to 43° using the Intelsat satellite (Greve, priv. com.).

At 340 GHz and 30 deg elevation, the fitted curve shows a drop of the aperture efficiency to 68% of the optimum value. The drop is stronger than expected from the measurements done on 31-Aug-2007 (Fig. 6, which indicated a drop to only 83%. These results should be compared with the results of finite element (FE) calculations of the backstructure (BUS), which are thought to be accurate to within 15% (Greve, priv. comm.).

One possible explanation is an observed degradation of the lateral focus (Fig. 3), possibly caused by the sun, as the low elevations were observed during sun rise. The sun may also have led to the observed broadening of the beam (see further below).

Figure 7 shows the surface rms derived from the aperture efficiencies observed at 145 GHz with E1 and at 340 GHz with E3, using the Ruze formula. The total rms near the optimum elevation is $64\,\mu$m. Within the errors, this compares well with the $60\,\mu$m surface rms derived on 31-Aug-2007, from observations at 86, 145, 210, and 260 GHz.

Using the fitted rms value with the Ruze formula, the aperture efficiency at zero frequency can be derived, for the different elevations (Fig. 8). Surprisingly, it is not constant but variies almost monotously between 63% and 68%. This may be another indication of a changing lateral focus.

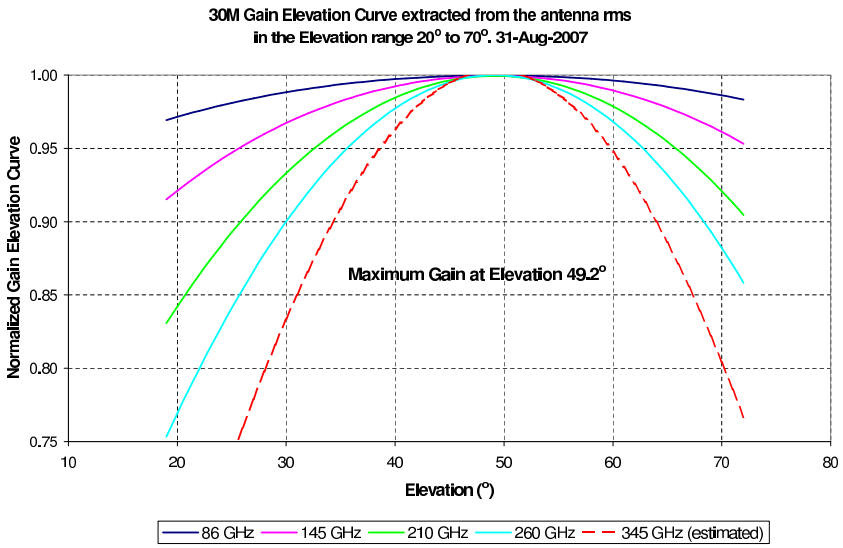

Figure 6: For comparison, gain elevation curves at 86, 145, 210, 260 GHz, fitted to the observations of 31-Aug-2007, and extrapolated to 345 GHz.

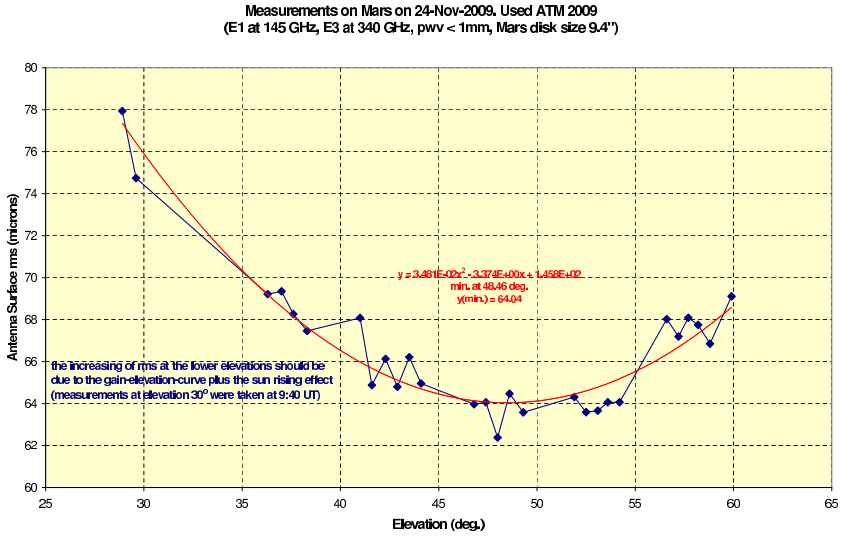

Figure 7: Surface accuracy derived from the Ruze formulae from the 2 mm and 0.9 mm data of 24-Nov-2009.

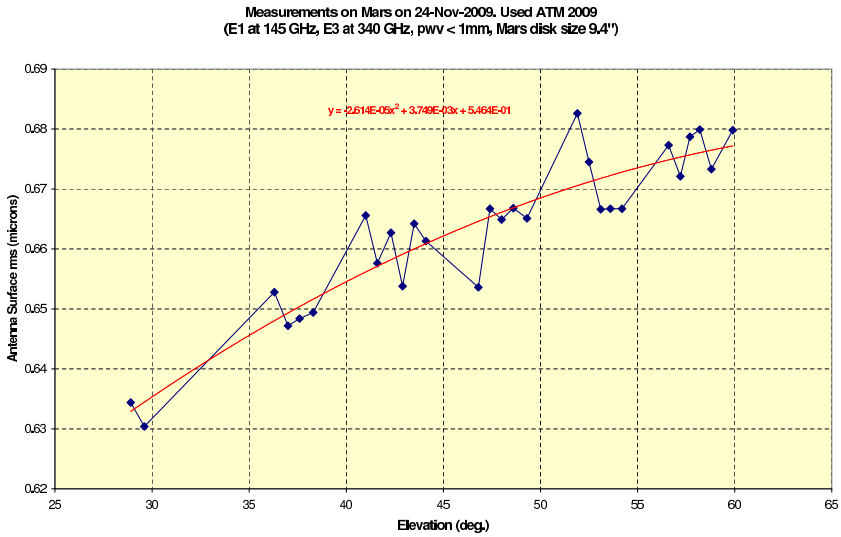

Figure 8: $A_{\mathrm{eff},0}$, at zero frequency, derived from the Ruze formula, vs. elevation.

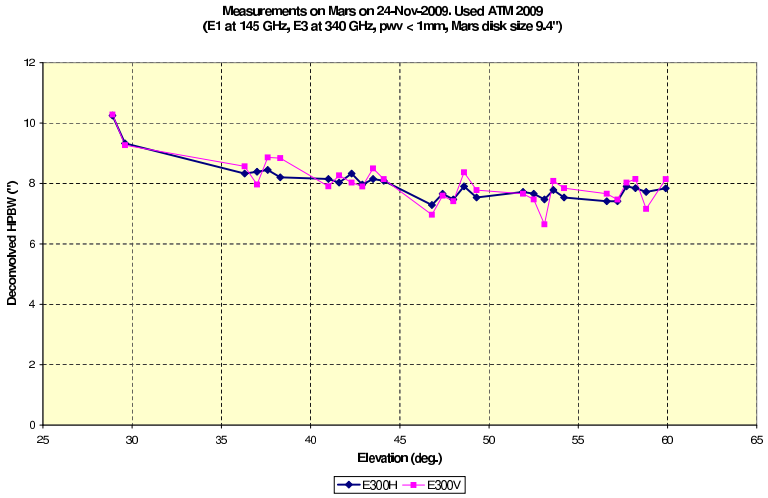

Figure 9: Half power beam width (HPBW) at 340 GHz for both polarisations vs. elevation. We find a broadening of the beam at low elevations.

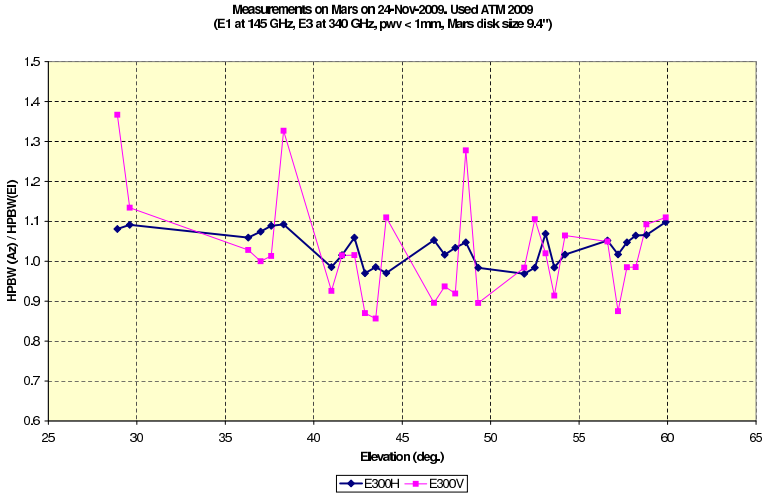

Figure 10: Ellipticity of the beam at 340 GHz vs. elevation. At low and at high elevations, the beam is slightly elliptical.

2.4 Half power beam widths

Figure 9 show the variation of the beam width with elevation. We find a broadening of the beam at low elevations, from $\sim 7''$ near the optimum elevation to $\sim 10''$ at 30° elevation.

The ratio of beam widths measured at Azimuth and Elevation, the beam ellipticity, is shown in Figure 10. The vertical polariation is much more noisy than the horizontal polarisation, as discussed further below. There is a slight increase of the ellipticity, from circular (1.0) near the optimum elevation to $\sim 10\%$ (1.1) at 30° elevation.

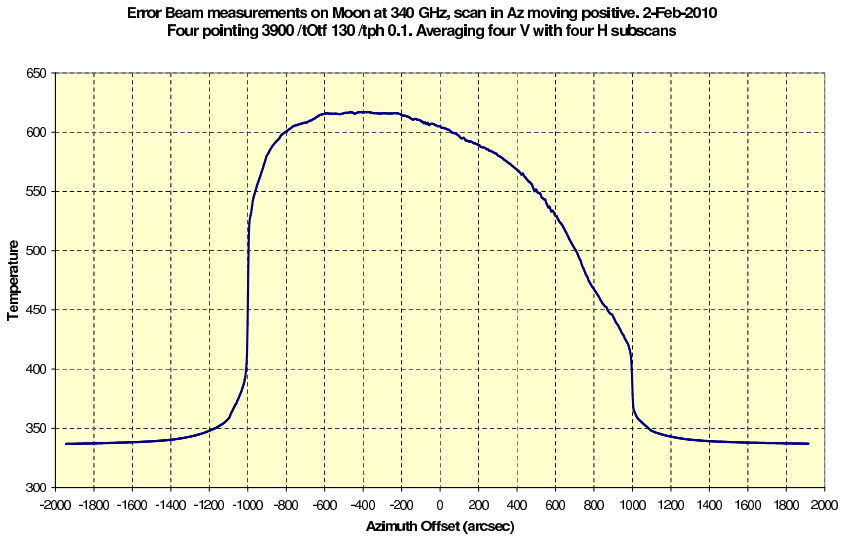

Figure 11: Moon scan at 340 GHz.

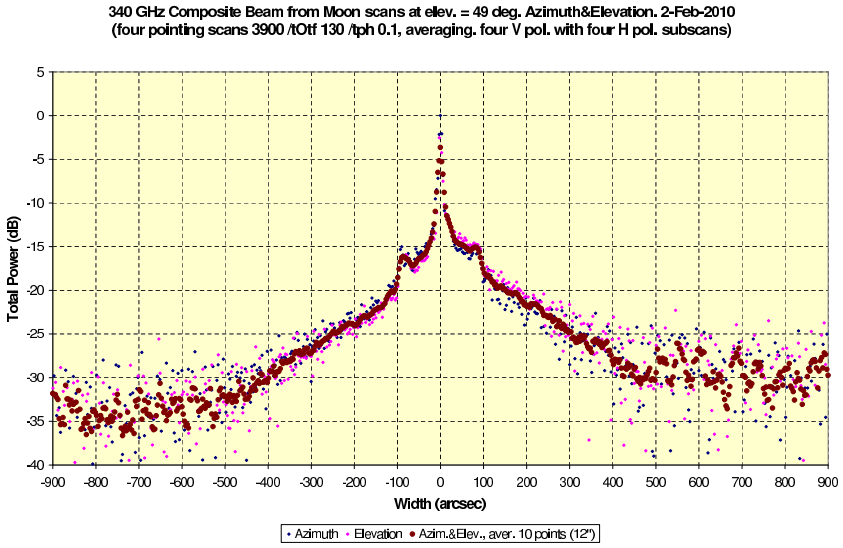

Figure 12: Differentiated Moon limb scan at 340 GHz.

2.5 Errorbeams

Lunar edge observations were conducted in 02-Feb-2010 (Fig. 11), only three days after full moon, under very good weather conditions (pwv=1.2 mm), during the night time hours 2:00 to 5:00. Cross scans of $3900''$ length were conducted at 86, 145, 210, 280, and at 340 GHz (cf. log100201.odt). Composite beams are constructed by differentiating these total power scan across the lunar edge. Note that these are not exactly the beam profiles.

Figure 12 shows the differentiated lunar profile (the ”composite beam”) at 340 GHz. It shows the main beam, errorbeams, and the diffraction rings. The sidelobes of the primary dish are expected next to the main beam, but are not seen, as they are not resolved. The right side of the composite beam is affected by the structure of the lunar surface, about 3 days after full moon, and should be ignored.

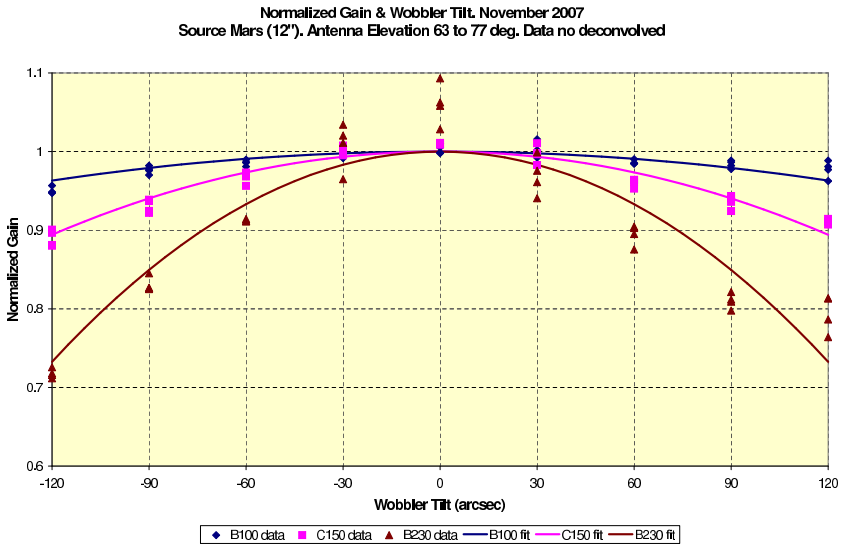

Figure 13: Normalized axial gain vs. wobbler throw, for 0 deg wobbler rotation

Near $100''$, a diffraction ring shows-up, staying below -15 dB. This is due to panel buckling, a transient effect, as described in a recent paper by Greve et al. (2010).

A more quantitative analysis, listing the power of the errorbeams, is in preparation. Note that polarisation affects the Moon emission at the limb and extends over a region of several tens arcseconds (Thum et al. 2003). This effect was not taken into account here.

2.6 Wobbler throw

The loss of axial gain with wobbler throw is shown in Figure 13. It shows antenna temperatures measured on Mars in 2007, for the three lower wavelength bands. Observations with E3, are yet missing. See also Greve et al. 1996.

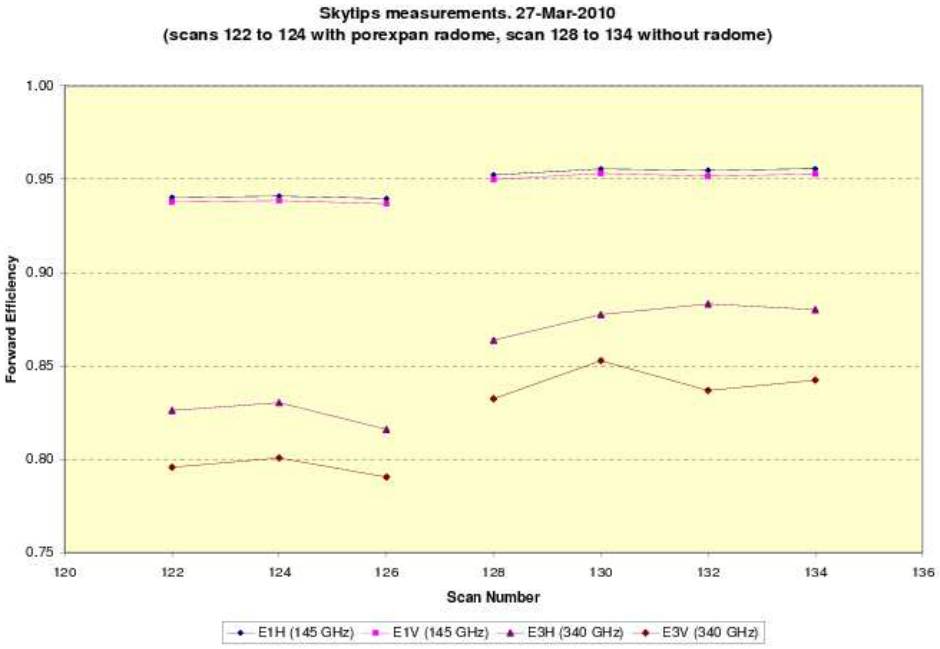

Figure 14: Improvement of forward efficiencies derived with and without the vertex membrane in place.

2.7 Membrane losses

The Vertex porexpan radome has an insertion loss of 7.3% at 340 GHz, as measured on 16-Feb-2010.

Skydips obtained with and without membrane, confirm this loss. Forward efficiencies determined from skydips on 27-Mar-2010, show an improvement by 6% from 81% to 86% at 340 GHz, when not using the membrane (Fig. 14). Note that the horizontal polarisation shows slightly higher forward efficiencies than the vertical polarisation. This effect had not been observed in previous measurements done on 24-Nov-2009.

The absorption by the vertex membrane, cannot lead to an increase of receiver temperature, as this is measured with hot & cold loads inside the cabin. The absorption by the membrane, does lead to an increase of the measured sky and system temperature. This leads to an increase of the forward efficiency.

However, this loss does not affect the antenna temperatures or the aperture or main beam efficiencies, as these are differential measurements. Formally, the forward efficiency $F_{\rm eff}$ cancels out when deriving the aperture efficiency $A_{\rm eff}$ from the peak antenna temperature T_A^* (delivered by odp/mira):

The relation between T_A^* and the aperture efficiency is:

$$T_A^* = \frac{S_{\rm pb} A_{\rm eff}}{F_{\rm eff} 2k}$$

with the flux per beam $S_{\rm pb}$. And T_A^* is calculated (by odp/mira) via:

$$T_A^* = \frac{(1+G_{\rm im})}{(F{\rm eff} * \exp(-\tau * A))} \times (T{\rm hot} - T_{\rm cold}) \frac{(C_{\rm on} - C_{\rm off})}{(C_{\rm hot} - C_{\rm off})}$$

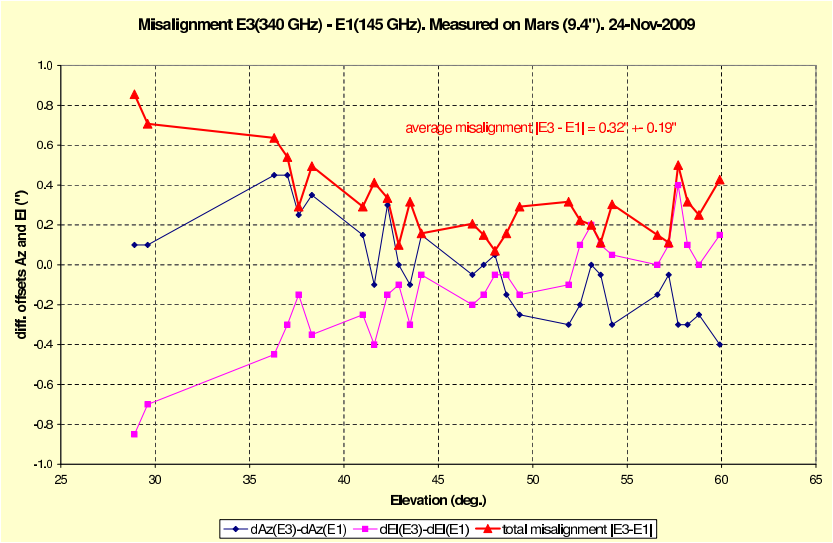

Figure 15: Alignment between E3 and E1, vs. elevations. Note the y-scale, which is ± 1 arcsec only.

2.8 Alignment with E1

Figure 15 shows the alignment between E1 and E3 for different elevations, as observed on Mars, 24-Nov-2009. The average alignment and rms are excellent: $0.3 \pm 0.2''$. This confirms the previous measurement, done on 29-Oct-2009, which had resulted in $0.75'' \pm 0.25''$.

2.9 Focus differences

The focus difference between E1 and E3 is:
focus(E3) = focus(E1) - 0.21 mm $\pm$ 0.02 mm,
from six good quality focus scans on Mars on 24-Nov-09.

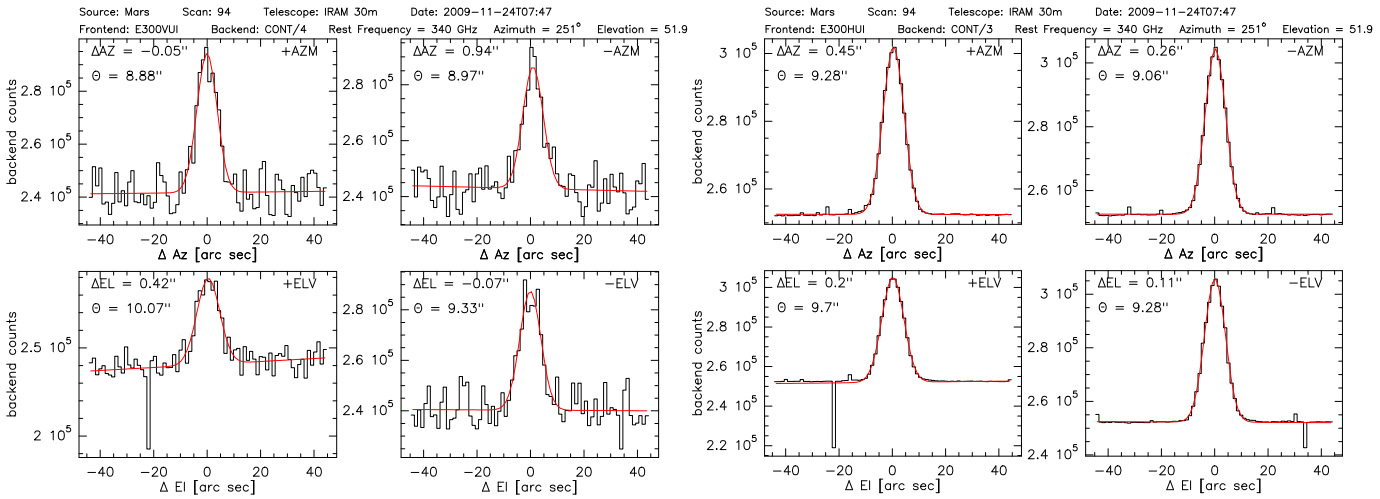

Figure 16: Left: Mars data taken with the Vertical polarisation in total power mode, showing excess noise, and negative spikes. Right: Mars data taken with the Horizontal polarisation in total power mode, showing much less noise than the Vertical polarisation shown above and taken simultaneously. Note the negative and positive spikes, but note also that this is one of the worst examples, concerning the spikes.

2.10 Noise

The noise of the Vertical polarisation is higher than for the Horizontal polarisation (Fig. 16). Continuum total power observations occasionally show jumps, in both polarizations simultaneously.

Continuum data also shows negative spikes, showing up simultaneously in both polarisations (Fig. 16), and ocassionally, weaker, positive spikes. The spike length is 100 msec or less.

3 Spectroscopic observations

Observations of two Galactic massive star forming regions (DR21, W51D) were carried out at 270, 280, 290, 300, 310, 320, 330, 345 GHz (BO, 20-Nov-09), partly under excellent weather conditions. Observations were conducted switching with the wobbler, in frequency, and in position. The backends WILMA, 4 MHz, and VESPA were used. Observations were done with E1 tuned to CS 3–2 in parallel to E3.

- All wobbler switched spectra have been viewed and they do not show obvious problems, in particular no line shifts or indications for spurious spikes (parasites).
- Spectral lines have been identified using a new line catalog provided by P. Schilke (Fig. 17).
- Spectra of both polarisations do not show any significant difference in noise. This was checked between 310 and 270 GHz.
- Receiver temperatures measured with the 4 MHz backend, after tuning by the operators, vary rather smoothly between 140-120 K at 345 GHz and 80 K at 270 GHz.

4 References

- Baars 2007, ”The Parabolical Reflector Antenna in Radio Astronomy and Communication”

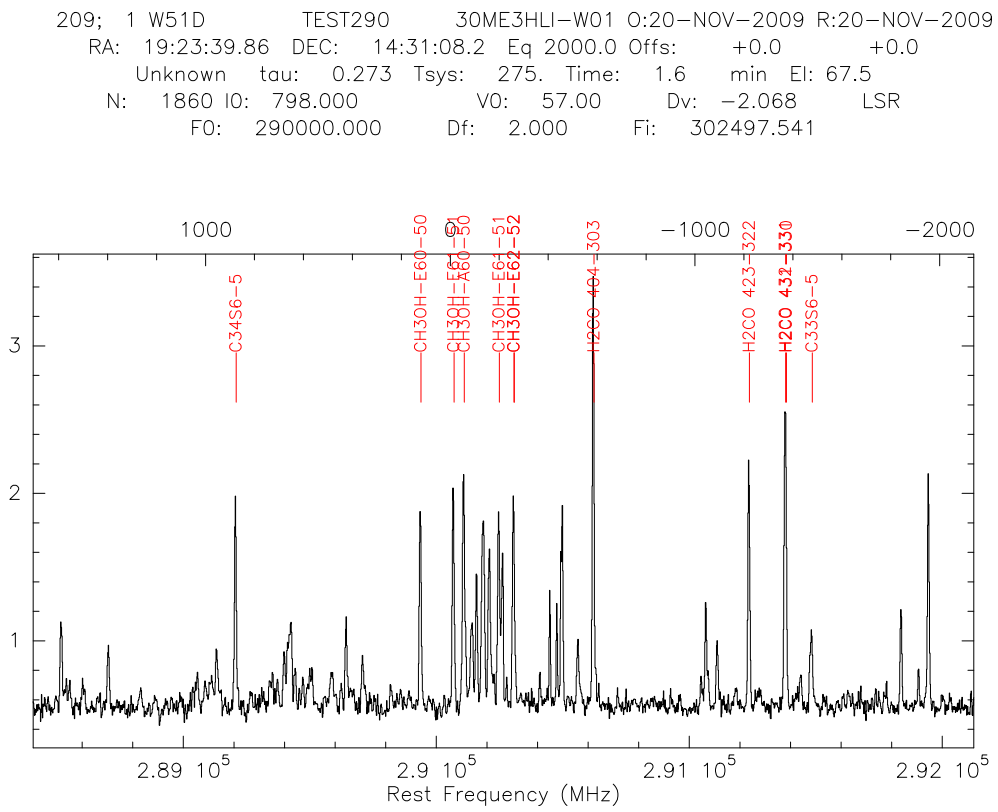

Figure 17: 4 GHz wide spectrum centered on 290 GHz, taken on W51D, using E3 and the 4MHz backend, wobbler switching.

- Greve, Baars, Penalver, leFloch 1996, Radio Science, ”Near-focus active optics: an inexpensive method to improve milllimeter-wavelength radio telescopes”, 31, 1053
- Greve et al. 2010, IEEE, “The Beam Pattern of Reflector Antennas with Buckled Rectangular Panels”
- Thum et al. 2003, “Versatile IF polarimeter at the IRAM 30m telescope”, Polarimetry in Astronomy. Edited by Silvano Fineschi . Proceedings of the SPIE, 4843, 272

For a list of calibration related 30m papers and technical report, please visit `http://www.iram.es/IRAMES/mainWiki/CalibrationPapers`.